

# Atomically Precise Transformations and Millimeter-Scale Patterning of Nanoscale Assemblies by Ambient Electrospray Deposition

Anirban Som, Depanjan Sarkar, Sisira Kanhirathingal, and Thalappil Pradeep\*

The performance of semiconductor devices can be fine-tuned through chemical transformation of their nanostructured components. Such transformations are often carried out in controlled conditions. Herein, the use of electrospray deposition of metal ions from solutions in air is reported, to bring about chemical transformations across mm<sup>2</sup>-sized areas of nanostructures. This is illustrated with monolayer assemblies of ultrathin tellurium nanowires (NWs). The process does not require any reducing agent and can transform the NWs chemically, in the solid state itself, under ambient conditions. By using suitable masks, the beam of ions can be patterned to localize such transformations with nanometer precision to obtain aligned multiphase NWs, containing atomically precise phase boundaries. By controlling the time of exposure of the spray, the scope of the process is further expanded to produce tellurium-metal telluride core-shell NWs. The method described here represents a crucial step for ambient processing of nanostructured components, useful for applications such as semiconductor device fabrication.

Spatial localization of chemical transformations is one of the focal points of semiconductor industry.<sup>[1]</sup> Imparting such transformations at the nanometer length scale is achieved through a variety of high-vacuum instrumentation involving multiple methods.<sup>[2,3]</sup> With rapid advances in solution-phase methods for nanoparticle (NP) synthesis, adaptable ambient protocols for their localized transformations would be a step toward processing of nanostructured components.

Here, we show that nanowires (NWs) can be transformed locally with the precision of one atomic layer by ambient electrolytic spray/electrospray deposition, methods involving spraying of metal ions from solution. Combined with the accessibility of large areas to impart effective transformations and with the ability to pattern the spray at will with nanometer precision would make this method promising for selective transformation of nanostructures.

Chemical transformations via electrospray deposition were demonstrated using ultrathin and ultrahigh aspect ratio trigonal

tellurium NWs (t-Te NWs), synthesized in solution. Solution processability of Te NWs adds an additional advantage toward low-cost manufacturing, essential for large-scale applications.<sup>[4,6]</sup> Tellurium and metal tellurides are low bandgap semiconductors and are materials of interest in thermoelectrics,<sup>[7,8]</sup> photovoltaics,<sup>[9]</sup> radiation detection,<sup>[10]</sup> etc. NWs of these materials exhibit enhanced or unique properties like high thermoelectric efficiency and photoconductivity<sup>[11,12]</sup> compared to their bulk counterparts due to altered and directional electrical and thermal conductivities.<sup>[13]</sup> Combined with anisotropic structure, compatibility of NWs with flexible substrates has resulted in high piezoelectric power harvesting efficiency.<sup>[14,15]</sup> These are also excellent templates for creating functional 1D nanomaterials.<sup>[16–19]</sup>

Localized transformations of Te NWs were performed on thin films of assembled NWs. Aligned monolayers of Te NWs were prepared at the air–water interface.<sup>[20]</sup> The process involves slow drop-casting of a butanolic dispersion of the Te NWs on top of the surface of water (Figure 1A). As 1-butanol quickly spreads on the surface of water, a temporary butanol–water bilayer is formed. The NWs also get dragged along with the flow and remains trapped in this thin layer of butanol. Evaporation of butanol from this layer increases the concentration of NWs, bringing them close to each other. These NWs then become aligned due to capillary forces, forming a monolayer assembly, which floats at the air–water interface. The aligned monolayer of pristine Te NWs was transferred onto carbon-coated copper grids used for transmission electron microscopy (TEM). These supported films were used for electrospray deposition of metal ions (Figure 1A). The large-area TEM image taken from one such grid (Figure 1B) shows a single layer of ultrathin Te NWs aligned along their major axis while the EDS spectrum (inset a, Figure 1B) confirms their chemical nature. The HRTEM image (Figure 1C) reveals (001) directed growth of the single crystalline Te NWs with trigonal crystal structure. The amount of Te per unit area of the grid was calculated from the population density and average diameter (8 nm) of the Te NWs.

Electrolytic spray deposition is a combination of two different processes; electrochemical corrosion and dissolution of a noble metal in an aprotic solvent, followed by electrospray deposition of the solvated metal ions. A nanoelectrospray source

Dr. A. Som, D. Sarkar, S. Kanhirathingal, Prof. T. Pradeep  
DST Unit of Nanoscience (DST UNS) and Thematic  
Unit of Excellence (TUE)  
Department of Chemistry  
Indian Institute of Technology Madras  
Chennai 600 036, India  
E-mail: pradeep@iitm.ac.in

DOI: 10.1002/ppsc.201700101

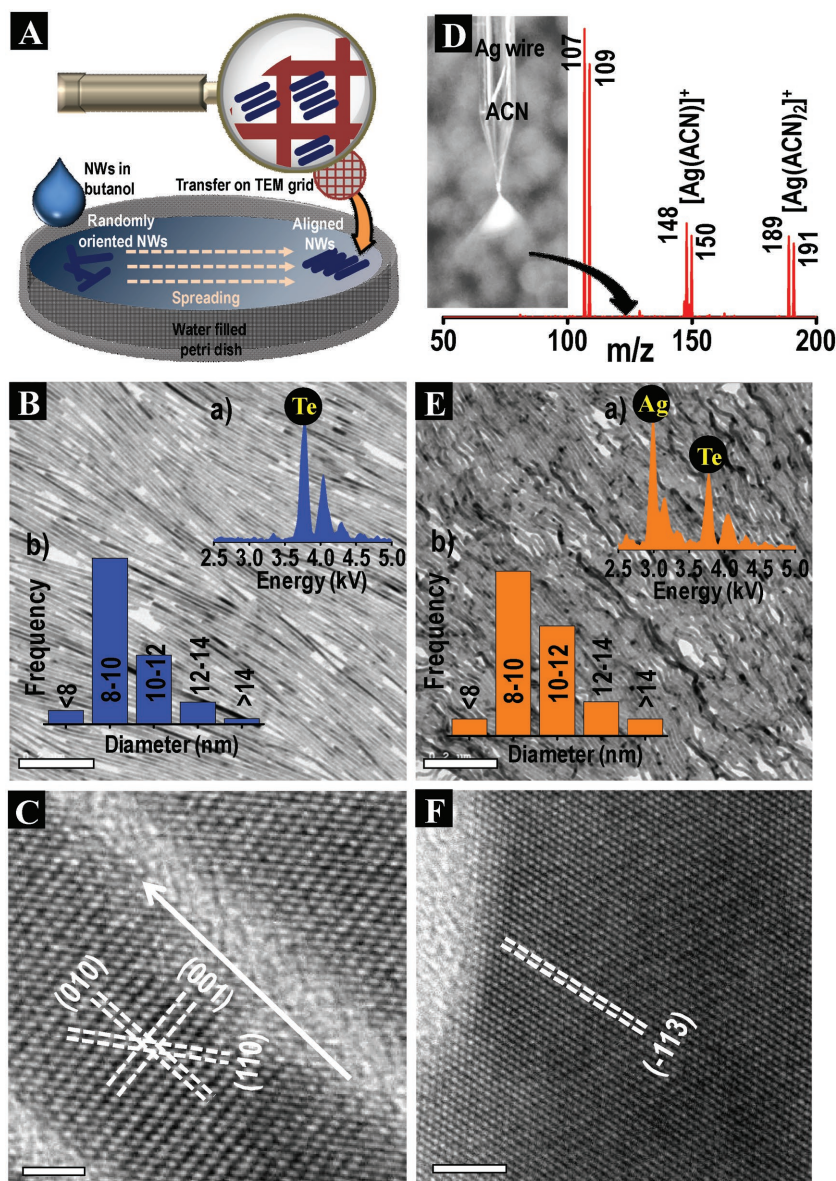


**Figure 1.** A) Schematic of the process of the formation monolayer assembly of Te NWs. Slow drop-casting of a butanolic dispersion of Te NWs on static water surface leads to the formation of aligned NWs on the liquid which is transferred on TEM grids and examined. B) Large-area TEM image of aligned monolayer of Te NWs. EDS spectrum is shown in inset a, while inset b represents the diameter distribution of the NWs. C) HRTEM image of the Te NWs, showing their *c*-axis directed growth and single crystalline nature. Lattice planes are marked. D) Mass spectrum showing the presence of  $\text{Ag}^+$  and solvated  $\text{Ag}^+$  ions in the electrolytic spray plume. A photographic image of a nanoelectrospray emitter during the spray process is shown in the inset. The tip of the Ag-electrode and the ejected ion plume is visible. E) Large-area TEM image of the monolayer of curly  $\text{Ag}_2\text{Te}$  NWs, converted through electrolytic spray deposition. EDS spectrum in inset a confirms the composition. Increase in diameter due to metal incorporation in the transformed NWs can be seen in inset b. F) HRTEM image of a single  $\text{Ag}_2\text{Te}$  NW. Single crystallinity of the NWs is retained during the transformation. Lattice plane is marked. Scale bar is 200 nm in (B) and (E) and is 2 nm in (C) and (F).

fitted with a metal wire works as the ion source. A high voltage ( $>1$  kV) was applied to a silver anode dipped in a solvent and a fine ion source was formed (inset, Figure 1D). It is important that anhydrous acetonitrile (ACN) is used as the solvent. The ejected electro-spray plume revealed the presence of free and

solvated silver ions (Figure 1D). Collection of such electro-spray plume has been shown to form catalytically active NPs on conductive surfaces<sup>[21]</sup> and the ion-beam can be patterned to obtain surface enhanced Raman scattering (SERS) active substrates.<sup>[22]</sup>

In our experiments, we landed this jet of solvated  $\text{Ag}^+$  ions onto the TEM grid, with a monolayer of Te NWs transferred onto it, by the process described earlier. The grid was electrically grounded and was then irradiated with  $\text{Ag}^+$  ions for a calculated amount of time, required for complete conversion of Te into  $\text{Ag}_2\text{Te}$ . The grounding procedure and measurement of the ion current are explained later in the manuscript. Distance of the electrolytic spray tip from the grid is an important parameter in this deposition process as the area of irradiation increases with increasing the tip to substrate distance, due to diverging nature of the plume (inset, Figure 1D). This distance was optimized through a blank experiment by carrying out electrolytic deposition of ions on a stainless-steel (SS) mesh. Nanoparticles formed by this ambient deposition method appear as a dark circle on the SS mesh and the area of irradiation for that particular tip to substrate distance was calculated by measuring the diameter of the circle (Figure S1, Supporting Information). The ion deposition time was calculated by evaluating the amount of Te present under the area of ion irradiation and rate of silver deposition. Concentration of silver ions in the plume was determined from the flow rate of ACN and the ion current.

Examination of the grid following electrolytic spray deposition revealed morphological changes in the NWs. The NWs, although retained their 1D morphology and alignment, became curly (Figure 1E). No sign of formation of silver nanoparticles was found, even on closer inspection, indicative of Ag metal incorporation in the Te NWs, to account for the silver dose. EDS analysis verified the composition of the formed NWs to be silver telluride (inset a, Figure 1E). Average diameter of the NWs following silver deposition increased by 33%, on par with the increase in diameter reported upon conversion of Te nanorod (NR) to  $\text{Ag}_2\text{Te}$  NR, in solution phase reaction.<sup>[23]</sup> Crystal structure of the transformed  $\text{Ag}_2\text{Te}$  NWs was determined by HRTEM analysis (Figure 1F).

The observed interplanar distance matches with  $(-113)$  plane of monoclinic  $\beta\text{-Ag}_2\text{Te}$ , the stable phase of  $\text{Ag}_2\text{Te}$  at room temperature.<sup>[24]</sup> Preservation of crystalline nature of the NWs stems from topotactic lattice matching between the t-Te and  $\beta\text{-Ag}_2\text{Te}$  phases.<sup>[23]</sup> HRTEM imaging and powder XRD pattern

of these transformed NWs (Figure S2A,B, respectively, Supporting Information) confirmed that the chemical transformation takes place uniformly throughout the entire volume of the NWs and a single  $\text{Ag}_2\text{Te}$  phase (monoclinic, JCPDS No. 34-0142) is formed. XPS analysis further confirmed the composition of  $\text{Ag}_2\text{Te}$  for the formed NWs. A small shift in the binding energy accompanied the broadening of the  $\text{Ag}3d$  peaks. Moreover, absence of the loss features to higher binding energy side of each spin-orbit component observed for metallic silver clearly indicated the presence of  $\text{Ag}(\text{I})$  (Figure S2C, Supporting Information). A shift in binding energy of  $\text{Te}3d$  peaks to lower values from the  $\text{Te}$  NWs also confirmed the formation of a telluride (Figure S2D, Supporting Information). However, the chemical transformation of  $\text{Te}$  into  $\beta\text{-Ag}_2\text{Te}$  results in large volume increase ( $\approx 100\%$ ) and transformed  $\text{Ag}_2\text{Te}$  NWs became bent/curly to release the strain induced by this large volume change. Such curling up of the nanowires was not observed when such transformation ( $\text{Te}$  to  $\text{Ag}_2\text{Te}$ ) was brought about in solution by adding an aqueous  $\text{Ag}^+$  solution into  $\text{Te}$  NW dispersion.<sup>[25]</sup> Monolayer assembly of such preformed  $\text{Ag}_2\text{Te}$  NWs is shown in Figure S3 (Supporting Information). However, the nanowires broke into smaller pieces ( $2\text{--}3\ \mu\text{m}$  from  $>10\ \mu\text{m}$ ) to release the strain. In the case of  $\text{Te}$  NWs already attached to a solid substrate, release of strain through a similar mechanism was not observed. Bending of the NWs at different locations, however, releases part of this strain, resulting in a curly morphology of the transformed NWs.

XPS, as well as thorough TEM analysis, of the resultant NWs did not show the presence of any  $\text{Te}(\text{IV})$  phase in the transformed sample. This eliminates the possibility of disproportionation of  $\text{Te}$  into  $\text{TeO}_3^{2-}$  and  $\text{Te}^{2-}$  in the presence of  $\text{Ag}^+$ . Electrolytic spray deposition of silver ions on grounded TEM grids leads to the formation of  $\text{Ag}$  NPs (Figure S4, Supporting Information).<sup>[21]</sup>  $\text{Ag}^+$  ions from the spray reach the grid surface, get neutralized, and form  $\text{Ag}$  NPs. The  $I\text{--}V$  curve, measured for a monolayer of  $\text{Te}$  NWs (Figure S5, Supporting Information) showed them to be electrically conducting. So,  $\text{Ag}^+$  ions from the spray can neutralize on surface of electrically grounded  $\text{Te}$  NWs and subsequently penetrate into the  $\text{Te}$  lattice, eventually forming the  $\text{Ag}_2\text{Te}$  phase.<sup>[26]</sup> The amount of silver deposited is crucial in achieving the final stoichiometry of the product. The formation of  $\text{Ag}_2\text{Te}$  is facilitated by the negative free energy of the process (as can be inferred from the solubility product  $> 10^{-54}$ , of  $\text{Ag}_2\text{Te}$ <sup>[23]</sup>). Electrolytic deposition of silver ions on preformed  $\text{Ag}_2\text{Te}$  NW monolayer, in contrast, resulted in the formation of  $\text{Ag}$  NPs on the NWs instead of further metal incorporation (Figure S6, Supporting Information).

As the solvated  $\text{Ag}^+$  ions are deposited in a spray deposition method, a suitable perforated mask can be placed in the path of the beam to selectively block parts of the beam. The remaining parts of the beam can then be used to bring about area-specific chemical transformation. We used both conducting (metal plate) and nonconducting (microscope cover glass or Teflon tape) substrates as masks and similar results were obtained in both the cases. **Figure 2A** shows a schematic representation of the masking and electrolytic spray deposition process where a microscope cover glass was used to cover half of a TEM grid coated with monolayer of  $\text{Te}$  NWs. The grid was electrically grounded by placing it on an indium tin oxide (ITO)-coated

glass slide, which was grounded through a picoammeter. The picoammeter measured the ion-deposition current. The cover glass was placed perpendicularly to the direction of alignment of  $\text{Te}$  NWs. Inspection of the grid post-deposition showed darker contrast for the NWs in the silver-deposited region of the grid, than in the covered region (Figure 2B). The chemical compositions of the light and dark regions of the NW monolayer were confirmed to be  $\text{Te}$  and  $\text{Ag}_2\text{Te}$ , respectively revealed by the EDS spectra taken from those regions (insets a and b, Figure 2B). The enhanced contrast in TEM for the silver-deposited region is on par with the increase in diameter of  $\text{Ag}_2\text{Te}$  NWs, compared to the  $\text{Te}$  ones. The  $\text{Te}$  section of the NW monolayer remained straight while  $\text{Ag}_2\text{Te}$  regions showed characteristic curly nature. Combined EDS map (image b, Figure 2C) for  $\text{Ag}$  and  $\text{Te}$  from such a region (image a, Figure 2C) confirmed the presence of  $\text{Ag}$  only within the darker region (image c, Figure 2C) while  $\text{Te}$  was present throughout (image d, Figure 2C). A high-magnification TEM image taken from a junction of the  $\text{Te}\text{--}\text{Ag}_2\text{Te}$  confirmed the coexistence of both the phases in a single NW with an atomically sharp phase boundary, perpendicular to the wire axis. It also confirmed the topotactic transformation of (001) directed  $\text{t-Te}$  into ( $-113$ ) directed  $\beta\text{-Ag}_2\text{Te}$  during the incorporation of  $\text{Ag}$  to form an axial nanowire-heterostructure (NWHs). A 33% increase in diameter of the NWs during this chemical transformation can also be clearly observed from the image. Such regiospecific transformation with a suitably placed mask can produce aligned array of axial NWHs (inset, Figure 2D).  $\text{Ag}_{2-x}\text{Te}$  is n-type semiconductor while  $\text{Te}$  is p-type semiconductor. Therefore, this simple process can produce an array of p–n junctions under ambient conditions, which can be an important processing step toward semiconductor device fabrication.

Such chemical transformation can be brought about over larger areas by this process. A TEM grid without a carbon coating was used as a mask to demonstrate this point. Chemical transformation over a large area was probed with Raman spectroscopic imaging as TEM is inadequate to probe such large areas.  $\text{Te}$  NWs show a distinctive Raman feature at  $124\ \text{cm}^{-1}$  originating from the  $A_1$  mode of its lattice vibration (inset, Figure 2E).<sup>[27]</sup> This feature diminished as the  $\text{Te}$  NW is converted into  $\text{Ag}_2\text{Te}$  and a broad band appeared (inset, Figure 2F). An aligned monolayer of  $\text{Te}$  NWs was transferred to an ITO-coated glass slide and the grid was placed on top it before performing  $\text{Ag}^+$  ion deposition. A Raman spectral image constructed by the Raman feature of  $\text{Te}$  after removal of the mask showed different contrast for the covered and bare regions (Figure 2E). Covered regions appeared bright as the  $\text{Te}$  remained intact while the bare regions appeared darker due to conversion of the  $\text{Te}$  NWs into  $\text{Ag}_2\text{Te}$ . A complementary pattern was observed when the image was constructed using the  $\text{Ag}_2\text{Te}$  feature (Figure 2F).

Electrolytic deposition of other metals like  $\text{Au}$  and  $\text{Cu}$  is also possible with a similar set-up where a  $\text{Ag}$ -wire is replaced with that of  $\text{Au}$  or  $\text{Cu}$ , respectively. Although solvated monovalent cations ( $\text{Au}^+$  and  $\text{Cu}^+$ ) were found to be present in the spray in both cases, they reacted differently with the  $\text{Te}$  NWs. Deposition of  $\text{Au}^+$  resulted in the formation of  $\text{Au}$ -islands on  $\text{Te}$  NWs (**Figure 3A,B**). Poor solubility of  $\text{Au}$  in  $\text{Te}$  lattice probably

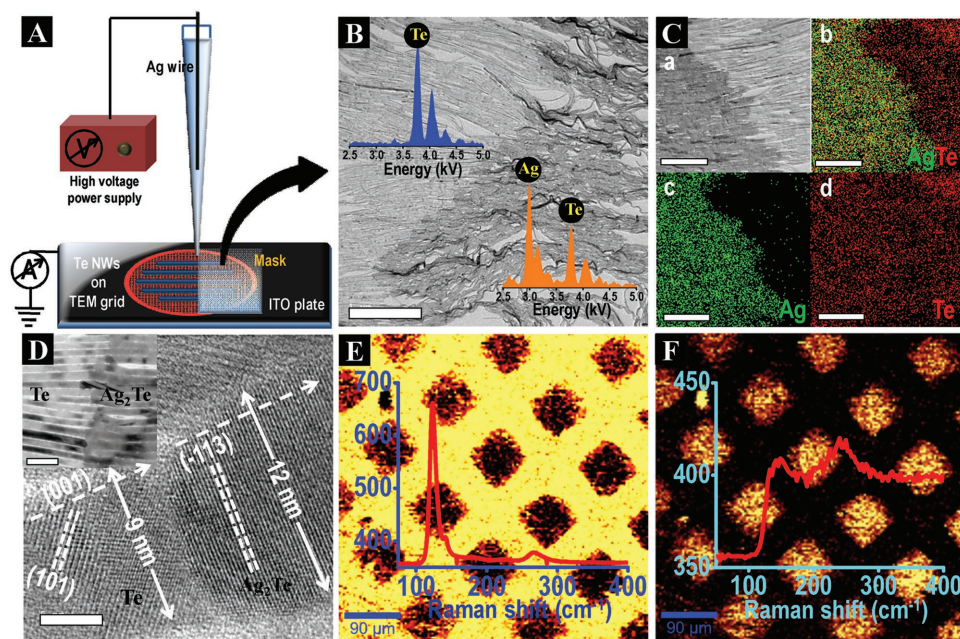


**Figure 2.** A) Schematic illustration of the electrolytic spray deposition of Ag on aligned Te NWs taken on a TEM grid. The masking process to achieve selective-area chemical transformation is also shown. B) A large-area TEM image from the junction of unmasked and masked area of the grid. The NWs in the masked area remained unmodified (inset a) while NWs from the areas exposed to the beam of  $\text{Ag}^+$  ion converted to  $\text{Ag}_2\text{Te}$  (inset b). The NWs from the exposed area became thicker and curly during the transformation. C) EDS mapping of the Te– $\text{Ag}_2\text{Te}$  junction region; a) TEM image of the region chosen for EDS mapping, b) Combined EDS map of Ag and Te intensities, c) Ag component map, and d) Te component map. The presence of Ag was restricted to the darker region in the TEM image while Te was present everywhere. This confirms the possibility of area-specific chemical transformation by using suitable masks. D) HRTEM image of single NW from the Te– $\text{Ag}_2\text{Te}$  junction showing the formation of biphasic heterojunction NWs at that region. The interphase between the t-Te and  $\beta\text{-Ag}_2\text{Te}$  was atomically sharp. Moreover, the measured diameters of the Te and  $\text{Ag}_2\text{Te}$  sections of the NW give a direct validation to the topotactic transformation of Te to  $\text{Ag}_2\text{Te}$ . Inset shows a lower magnification image of the junction showing the formation of an array of Te– $\text{Ag}_2\text{Te}$  NWs. E) Large-area intensity map of Raman feature of Te following silver deposition using an uncoated TEM grid as mask. The areas covered by the grid retained Te feature and appear bright but the exposed regions appear dark due to conversion into  $\text{Ag}_2\text{Te}$ . F) Raman image of the same area constructed using Raman feature of  $\text{Ag}_2\text{Te}$ . The image appears complementary to E for obvious reasons. Scale bar is 1  $\mu\text{m}$  in (B), 100 nm in (C), 3 nm in (D), and 100  $\mu\text{m}$  for (E,F). Scale bar for the inset in (D) is 50 nm.

is the reason for the formation of Au NPs. As metal deposition increases, the conductivity of the Te NWs increase and such structures can be used in flexible electronics.<sup>[28]</sup> Cu, on the other hand, reacts in a similar manner like Ag, and forms  $\text{Cu}_2\text{Te}$  NWs (Figure 3C). Composition and the phase formed were determined from the HRTEM image (Figure 3D).

The scope of electrolytic spray is restricted by the use of metallic wires, which are used as anodes, as well as the source of the metal ions in the process. However, electro spray is a more universal process where metal salts are dissolved in appropriate solvents and sprayed by applying high voltages. To check whether similar chemical transformation can be induced by electro spray deposition, a solution of silver acetate was electro sprayed using a platinum (Pt) wire as the anode. It is important to note that, in the case of Pt, electro corrosion was not observed, and that was the reason for its choice as anode for electro spray. Electro spray of silver acetate using water as solvent showed the presence of  $\text{Ag}^+$  in the plume (Figure S7A, Supporting Information). Collection on TEM grids resulted in the formation of Ag NPs and direct deposition transformed Te NWs into  $\text{Ag}_2\text{Te}$  NWs (Figure S7B, Supporting Information), much like in the case of electrolytic spray. Inspired by this phenomenon, we tried electro spray and induced chemical transformations of the Te NW monolayer for a variety of other

metals, which can potentially form metal telluride NWs, useful for applications. Optimized parameters used for electro spray deposition is given in the Experimental Section in the Supporting Information. Acetate was chosen as the counter anion of choice for these experiments due to solubility of metal acetates in a wide variety of solvents.

Electro spray deposition of Hg and Cd acetates was performed on monolayer assemblies of Te NWs taken on grounded TEM grids. TEM examination of the Hg deposited grids showed only the presence of aligned NWs (Figure 3E). EDS spectrum collected from these NWs showed the presence of both Hg and Te, revealing the incorporation of deposited mercury ions into the crystal lattice of the parent Te NWs (inset, Figure 3F). HRTEM taken from one of these NWs (Figure 3F) confirms the formation of crystalline HgTe phase. Similar electro spray deposition of Cd onto electrically grounded monolayer of Te NWs leads to incorporation of Cd keeping the morphology intact (Figure 3G). The HRTEM image (Figure 3H) confirms that the single-crystalline nature of the NWs was being retained during the Te to CdTe chemical transformation.

Electro spray deposition of Bi onto Te NWs (using bismuth acetate in methanol as a precursor) to convert them into  $\text{Bi}_2\text{Te}_3$ , however, resulted in a different phenomenon, different from the Cd and Hg cases. Deposition of Bi in this method

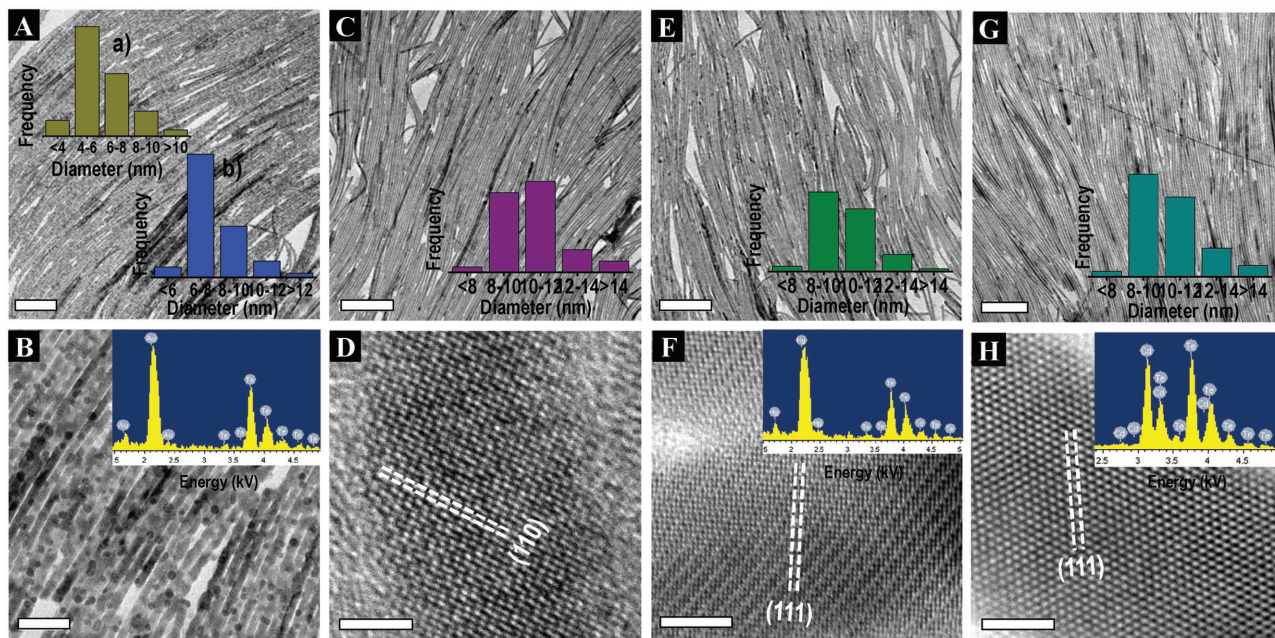


**Figure 3.** A) Large-area TEM image of electrochemically gold deposited Te NWs. B) A higher-magnification TEM image of the same showing nodular growth of NPs on the NWs. EDS spectrum (shown in the inset) confirms the presence of gold. Size distribution of the Au NPs and diameter distribution of the NWs is shown in the insets a and b, respectively in image A. C) Large-area TEM image of  $\text{Cu}_2\text{Te}$  NWs made by electrolytic deposition from a monolayer assembly of Te NWs. D) HRTEM image of a  $\text{Cu}_2\text{Te}$  NW which confirms the phase formation and single crystalline nature of the transformed NWs. E) Large-area monolayer assembly of HgTe NW formed through electro spray deposition. F) HRTEM image confirming the formation of HgTe. EDS spectrum (shown in the inset) indicated incorporation of Hg into Te. G) TEM image of aligned assembly of CdTe NWs obtained through ambient electro spray deposition. H) HRTEM image of a CdTe NW, confirming the formation of single crystalline NWs. EDS spectrum (inset) shows the integration of Cd into Te Lattice. Diameter distributions of  $\text{Cu}_2\text{Te}$ , HgTe and CdTe NWs are given in the insets of images (C), (E), and (G), respectively. Lattice planes are marked in the HRTEM images. Scale bar is 200 nm in images (A), (C), (E), and (G), 50 nm in (B), and 2 nm in (D), (F), and (H), respectively.

led to the formation of islands on the NWs and can be seen from the TEM image (Figure 4A). Chemical analysis of these darker islands through EDS revealed them to be bismuth oxide/hydroxide. The mass spectrum collected from the spray plume showed the presence of bismuth oxy cation ( $\text{BiO}^+$ ) with

higher intensity than  $\text{Bi}^+$  along with the presence of  $\text{Bi}(\text{OH})_2^+$  and  $\text{Bi}(\text{OMe})_2^+$  (inset, Figure 4A). These oxygen-containing Bi species accumulate on the NW surface in the course of the spray and form bismuth oxide/hydroxide islands. A TEM image of the NWs (after their redispersion and separation from other

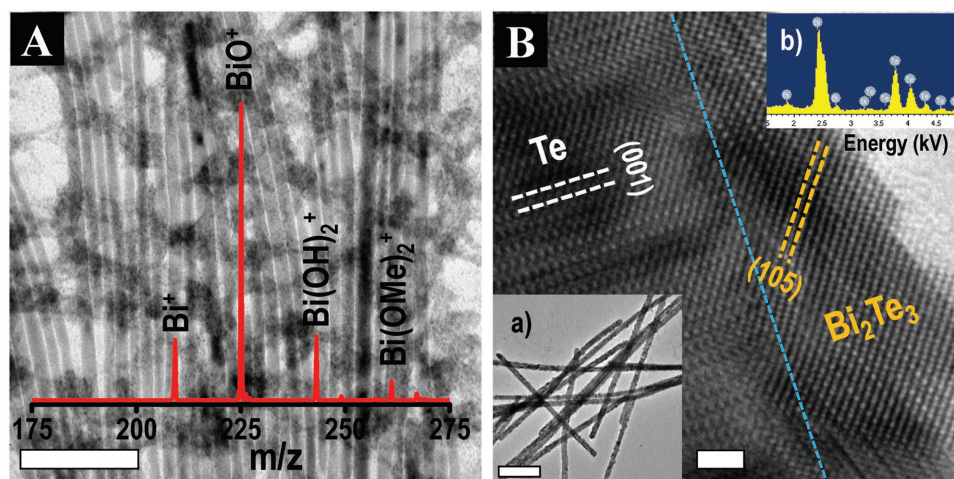


**Figure 4.** A) TEM image showing the formation of bismuth oxide on the NWs after electro spray deposition. Mass spectrum collected from an electro sprayed solution of bismuth acetate in methanol showing the presence of bismuth oxy cations along with  $\text{Bi}^+$  is shown in the inset. B) HRTEM image showing the formation of Te- $\text{Bi}_2\text{Te}_3$  core-shell NWs in the electro spray deposition process. Corresponding lattice planes are marked. Image was collected after removal of bismuth oxides through centrifugation. TEM image of these NWs is shown in inset a. EDS spectrum, shown in the inset b, confirms the presence of Bi in these NWs. Scale bar is 100 and 5 nm for images (A) and (B), respectively and 50 nm for inset of (B).

species by centrifugation, (Figure 4B, inset a) and the EDS spectrum collected from these NWs (Figure 4B, inset b) confirm the incorporation of Bi in them. HRTEM image of one such NW (Figure 4B) revealed these NWs to be Te–Bi<sub>2</sub>Te<sub>3</sub> core-shell NWs. The complete transformation of Te into Bi<sub>2</sub>Te<sub>3</sub> did not happen as the NW surface becomes covered with bismuth oxide/hydroxide after a certain deposition time and NW surfaces at this point became inaccessible for incoming Bi atoms, leading the formation of core-shell heterostructure NWs.

In summary, we report the use of the electrolytic deposition of metal ions to bring about localized, nanometer-resolved chemical transformation across mm<sup>2</sup>-sized areas of monolayer assemblies of ultrathin tellurium nanowires. This process does not require any special conditions and can transform the NWs chemically, directly in the solid state, under ambient conditions. By using suitable masks, the beam of ions could be patterned to localize such transformation with nanometer precision to obtain aligned hetero-nanowires. My mixing suitable metal salts to the spray solution, scope of the process was further expanded to produce a variety of metal telluride and tellurium-metal telluride core-shell NWs. The method described here represents a promising step for ambient processing of nanostructured components for semiconductor device fabrication.

## Supporting Information

Supporting Information is available from the Wiley Online Library or from the author.

## Acknowledgements

A.S. and D.S. contributed equally to this work. The authors thank the Department of Science and Technology, Government of India for constantly supporting the research program on nanomaterials. D.S. thanks UGC for a research fellowship.

## Conflict of Interest

The authors declare no conflict of interest.

## Keywords

1D nanowires, electrolytic spray, electrospray deposition, localized transformations, semiconductor heterostructures

Received: March 16, 2017

Revised: April 9, 2017

Published online:

- [1] M. Mahjouri-Samani, M.-W. Lin, K. Wang, A. R. Lupini, J. Lee, L. Basile, A. Boulesbaa, C. M. Rouleau, A. A. Puzos, I. N. Ivanov, K. Xiao, M. Yoon, D. B. Geohegan, *Nat. Commun.* **2015**, *6*, 7749.
- [2] A. Y. Cho, J. R. Arthur, *Prog. Solid State Chem.* **1975**, *10*, 157.
- [3] *Pulsed Laser Deposition of Thin Films*, (Eds: D. B. Chrisey, G. K. Hubler), Wiley, New York **1994**.
- [4] Y. Xia, P. Yang, Y. Sun, Y. Wu, B. Mayers, B. Gates, Y. Yin, F. Kim, H. Yan, *Adv. Mater.* **2003**, *15*, 353.
- [5] J.-W. Liu, H.-W. Liang, S.-H. Yu, *Chem. Rev.* **2012**, *112*, 4770.
- [6] N. P. Dasgupta, J. Sun, C. Liu, S. Brittman, S. C. Andrews, J. Lim, H. Gao, R. Yan, P. Yang, *Adv. Mater.* **2014**, *26*, 2137.
- [7] J. R. Sootsman, D. Y. Chung, M. G. Kanatzidis, *Angew. Chem., Int. Ed.* **2009**, *48*, 8616.
- [8] M. W. Gaultois, T. D. Sparks, C. K. H. Borg, R. Seshadri, W. D. Bonificio, D. R. Clarke, *Chem. Mater.* **2013**, *25*, 2911.
- [9] L. Kranz, S. Buecheler, A. N. Tiwari, *Sol. Energy Mater. Sol. Cells* **2013**, *119*, 278.
- [10] A. Rogalski, *Proc. SPIE* **2003**, 4999, 431.
- [11] Y. Wang, Z. Tang, P. Podsiadlo, Y. Elkasabi, J. Lahann, N. A. Kotov, *Adv. Mater.* **2006**, *18*, 518.
- [12] J.-W. Liu, J. Xu, H.-W. Liang, K. Wang, S.-H. Yu, *Angew. Chem., Int. Ed.* **2012**, *51*, 7420.
- [13] H. Peng, N. Kioussis, G. J. Snyder, *Phys. Rev. B: Condens. Matter Mater. Phys.* **2014**, *89*, 195206.
- [14] T. I. Lee, S. Lee, E. Lee, S. Sohn, Y. Lee, S. Lee, G. Moon, D. Kim, Y. S. Kim, J. M. Myoung, Z. L. Wang, *Adv. Mater.* **2013**, *25*, 2920.
- [15] T.-C. Hou, Y. Yang, Z.-H. Lin, Y. Ding, C. Park, K. C. Pradel, L.-J. Chen, Z. L. Wang, *Nano Energy* **2013**, *2*, 387.
- [16] H.-H. Li, S. Zhao, M. Gong, C.-H. Cui, D. He, H.-W. Liang, L. Wu, S.-H. Yu, *Angew. Chem., Int. Ed.* **2013**, *52*, 7472.
- [17] H.-W. Liang, J.-W. Liu, H.-S. Qian, S.-H. Yu, *Acc. Chem. Res.* **2013**, *46*, 1450.
- [18] M. Chhetri, M. Rana, B. Loukya, P. K. Patil, R. Datta, U. K. Gautam, *Adv. Mater.* **2015**, *27*, 4430.
- [19] H.-H. Li, S.-Y. Ma, Q.-Q. Fu, X.-J. Liu, L. Wu, S.-H. Yu, *J. Am. Chem. Soc.* **2015**, *137*, 7862.
- [20] G. D. Moon, T. I. Lee, B. Kim, G. S. Chae, J. Kim, S. H. Kim, J.-M. Myoung, U. Jeong, *ACS Nano* **2011**, *5*, 8600.
- [21] A. Li, Q. Luo, S.-J. Park, R. G. Cooks, *Angew. Chem., Int. Ed.* **2014**, *53*, 3147.
- [22] A. Li, Z. Baird, S. Bag, D. Sarkar, A. Prabhath, T. Pradeep, R. G. Cooks, *Angew. Chem., Int. Ed.* **2014**, *53*, 12528.
- [23] G. D. Moon, S. Ko, Y. Xia, U. Jeong, *ACS Nano* **2010**, *4*, 2307.
- [24] I. Karakaya, W. T. Thompson, *J. Phase Equilib.* **1991**, *12*, 56.
- [25] A. K. Samal, T. Pradeep, *J. Phys. Chem. C* **2009**, *113*, 13539.
- [26] Y. Yang, K. Wang, H.-W. Liang, G.-Q. Liu, M. Feng, L. Xu, J.-W. Liu, J.-L. Wang, S.-H. Yu, *Sci. Adv.* **2015**, *1*, e1500714.
- [27] A. S. Pine, G. Dresselhaus, *Phys. Rev. B* **1971**, *4*, 356.
- [28] J.-W. Liu, W.-R. Huang, M. Gong, M. Zhang, J.-L. Wang, J. Zheng, S.-H. Yu, *Adv. Mater.* **2013**, *25*, 5910.